

Article

Investigation and Analysis of Attack Angle and Rear Flow Condition of Contra-Rotating Small Hydro-Turbine

Ding Nan ^{1,3}, Toru Shigemitsu ^{2,*} and Shengdun Zhao ¹

¹ School of Mechanical Engineering, Xi'an Jiaotong University, Xi'an 710049, China; ndndnd1988@163.com (D.N.); sdzhao@mail.xjtu.edu.cn (S.Z.)

² Institute of Science and Technology, Tokushima University, Tokushima 770-8506, Japan

³ Graduate School of Advanced Technology and Science, Tokushima University, Tokushima 770-8506, Japan

* Correspondence: t-shige@tokushima-u.ac.jp; Tel.: +81-088-656-9742

Received: 10 June 2018; Accepted: 3 July 2018; Published: 10 July 2018



Abstract: At present, there is strong impetus for renewable energy to replace the traditional energy sources because of the environmental pollution. Small hydropower is a promising renewable energy source; however, small hydro-turbines easily become blocked and impacted, and the efficiency of such devices is lower. Therefore, we examined contra-rotating rotors to overcome these disadvantages. We have made modifications to the blade thickness and to the front hub of the original model. In this paper, we focus on the attack angle and rear flow condition of the original model and the modified one. The axial and circumferential velocities are given as outputs, from which the attack angle is then calculated. The results show that the attack angle of new model is smaller at the hub area. The stagnation point of the rear rotor was moved slightly to the pressure surface of the rear blade, and the separation at leading edge area was suppressed. The crowded flow at the tip clearance area is also reduced. The high turbulent kinetic energy area is moved forward to the middle of the blade. The rear rotor's torque is bigger and changes more smoothly. Therefore, the rear flow conditions of the new model are improved.

Keywords: renewable energy; small hydro-turbine; contra-rotating rotors; attack angle; flow condition

1. Introduction

Environmental pollution and the depletion of energy resources has been a severe problem for human society. Therefore, there is strong impetus for renewable energy to replace the traditional energy sources because of the environmental pollution. There are many kinds of renewable energy, such as hydro, wind and solar [1]. Small hydropower is considered to be promising despite the fact that it is not widely used.

The electrical energy which is generated by small hydropower generators can be directly connected to the distribution network and provide electrical power for users. Therefore, the cost of small hydropower generation is very low. Based on this characteristic, small hydropower generation systems can be installed in some remote areas. These areas include remote rural areas which are out of the service of national power system, or the remote areas which haven't joined the distribution network yet because of the high cost of the expansion of the grid. Small hydropower generation systems can also provide electrical power for small communities or some small factories, satisfying a part of the power demands at these places, and making them use the power generated from renewable sources.

With the background of serious environmental pollution and depletion of energy resources, many countries all over the world are advocating for environmental protection and energy saving.

Therefore, taking advantage of small hydropower resources will be an effective method to achieve environmental protection and energy saving. By means of designing improved small hydropower systems, the environmental problems can be alleviated, and economic benefits can also be obtained. Based on these factors, small hydropower systems are strongly supported by many countries all over the world.

There are a lot of power ranges for small hydropower equipment. For example, 100–1000 kW is widely used now. However, this power range needs foundation construction, which is harmful to the environment. There are also many places that can generate 0.1–1 kW, such as the water supplying system in farmlands or on small streams. These kinds of places don't need foundation construction, so that they are harmless for the environment. For this kind of small power range, Darrieus and gyro-type turbines are suitable because they are designed for low-head working environments. Therefore, the performance and optimizing of Darrieus and gyro-type turbines are investigated [2,3]. Darrieus hydro-turbines are suitable for extra-low-head working environments such as small streams. To protect the Darrieus hydro-turbine, a waste screening system upstream from the turbine is installed and tested [4]. Some additional structures such as inlet nozzles are investigated. The experiments and numerical results show that these innovations can help to enhance the performance of Darrieus hydro-turbine [5]. The spiral water turbine can achieve a wide flow passage and has little impact on the environment. Therefore, the internal flow condition of spiral water turbines is investigated [6]. The cross-flow turbine is also friendly to the environment and can be used in small streams. The cost of operating Savonius turbines is very low. At the same time, a shield plate to improve performance is considered, and the optimum position of the plate is reported [7–9].

There are two disadvantages for small hydro-turbines. One is that the efficiency of small hydro-turbines is lower. Another is the potential for problems due to foreign materials in the fluid media [10]. Such problems may be blockages in the rotor or the impact of the foreign materials on performance. It is important to ensure optimal internal flow conditions, i.e., free from foreign materials, and it is also necessary to obtain stability in the hydro-turbine. Therefore, contra-rotating rotors were chosen for study. This kind of structure has the potential to achieve a wide flow passage and stable running. Not only contra-rotating rotors can achieve a wide flow passage; however, the contra-rotating rotors can also achieve high efficiency, and such a structure is smaller and compact. Therefore, the contra-rotating rotor is suitable for the working environment.

Counter-rotating rotors have been the object of other studies; the performance of this kind of structure, the optimizing of blade solidity, and potential interference are discussed in these references [11–13]. The diameter of the contra-rotating, small hydro-turbine is only 60 mm, and this will make it difficult to manufacture the generator. To solve this problem, we concluded that installing two independent generators in the rotors is more suitable.

A new kind of support structure can be also designed and used in the contra-rotating tidal turbine to improve its performance [14]. The results of the research indicate that the support structure contributes significantly to the behavior of the turbine and to the turbulence levels downstream, even when the rotors are upstream. There are many kinds of support structures that can be used in small hydro-turbines. For example, the guide vane and the fairwater are commonly used. Guide vanes are always installed in front of and behind the rotor, where they can help unify the flow direction. This is important because it helps to decrease the vortex in front of the rotor and enhance the efficiency of the turbine. The fairwater is also an important support structure. Compared with the guide vane, the fairwater is far from the rotor; it can help to concentrate the flow in front of the rotor, thereby improving flow conditions and enhancing efficiency.

We refer to this compact hydro-turbine as a contra-rotating small hydro-turbine in our research. This device has high portability, and it can take advantage of small hydropower resources which are not presently being widely used.

We undertook some research in Tokushima Prefecture in Japan. We have chosen some places to make field tests, including testing of head, flow rate, water quality and capacity utilization [15].

To predict the performance of the turbine, a numerical simulation was conducted and the results demonstrate the application's feasibility [16]. Then, we established the experimental apparatus, and the original test turbine was manufactured for performance experiments. The numerical result is also used to clarify the internal flow conditions [17,18]. There are four spokes between front and rear rotor; the internal lose is generated because of the spokes. To decrease the internal lose, we changed the spoke shape from cuboid to conical, and the performance is highly improved [19]. After that, we continued to change the spoke from conical to cylindrical, and perform numerical analyses. The simulation result shows that the performance and internal flow conditions are further improved [20]. To clarify the running stability, we performed foreign materials experiments to evaluate performance when foreign vegetable materials become attached to the blade [21]. We designed and manufactured a new test turbine to enhance performance and improve the internal flow conditions of this contra-rotating small hydro-turbine [22]. The evaluation criteria for velocity distributions in front of bulb hydro turbines are also investigated [23]. We have changed the blade thickness and the shape of front rotor to establish the new test turbine, and we have also made performance experiments and numerical simulations. To compare with the original model, we investigated the differences between the new model and the original.

In this paper, we focus on the attack angle and rear flow conditions of the original and new models. Two planes which are vertical to the casing are created to obtain the value of the attack angle; these planes are located 3 mm upstream from the front rotor and 3 mm upstream from the rear rotor. In each plane, we established 6 points and outputted the axial velocity and circumferential velocity of that point. Then, we could calculate the attack angle of that point. We are also interested in the rear flow condition because a lot of evidence supports the hypothesis that the rear rotor is key for enhancing performance. Therefore, some differences in the rear flow condition between the original test turbine and new test turbine were observed and investigated.

2. Experimental Work

2.1. Basic Design Method of the Models

The assumed working environment of the small hydro-turbine is a water supplying casing in a farmland setting. The diameter of the casing is nearly 60 mm. The design flow rate is $Q_d = 4.825$ L/s. The design head is $H_d = 2.6$ m. These parameters are based on the assumed working environment. In this environment, the power is about $P_a = 10\text{--}100$ W, the head is about $H_a = 1\text{--}4$ m, and the flow rate is about $Q_a = 2\text{--}10$ L/s. We designed the head of the front and rear rotors in the same way. Therefore, the design head $H_{df} = H_{dr} = 1.3$ m. The power of the generator is about 10–100 W. Based on this power, the rotation speed is designed to be $N_f = N_r = 2300$ r/min.

The original test turbine is shown in Figure 1a. To make the size of the original test turbine clear, we put a mouse beside it. We designed the hub tip ratios of the front and rear rotors in the same way; they are $D_{hf}/D_{tf} = D_{hr}/D_{tr} = 0.5$. In order to suppress the interaction of the blade rows between the front and rear rotors, the blade numbers should be co-prime. Therefore, the front blade number is $Z_f = 4$, the rear blade number is $Z_r = 3$. We chose NACA65 (National Advisory Committee for Aeronautics, American government, USA) as the profile of the front and rear blades. We did not adopt the guide vane because we wanted the small hydro-turbine to be as compact as possible. The basic parameters of the original rotors are shown in Table 1. The new test turbine is manufactured by 3D printing; it is shown in Figure 1b.



Figure 1. The original test turbine and new test turbine of contra-rotating small hydro-turbine. (a) Original test turbine. (b) New test turbine.

Table 1. Basic parameters of the original model.

Rotor	Parameter	Hub	Mid	Tip
Front Rotor	Diameter (mm)	29	43.5	58
	Blade Number	4		
	Blade Profile	NACA65		
	Solidity	1.4	1.07	0.85
	Setting Angle (°)	25.5	20	15.8
Rear Rotor	Diameter (mm)	29	43.5	58
	Blade Number	3		
	Blade Profile	NACA65		
	Solidity	0.86	0.71	0.59
	Setting Angle (°)	44.6	29.7	18.9

Regarding the two test turbines, there are two differences between the original and the new model. One difference is about the shape of front hub. For the original model, the chamfer is a flat plane. For the new model, the chamfer is a curved surface. The curve is a part of an arc whose radius is 20 mm. The length of the new front hub is longer than the original front hub. The front rotor length of the original model is 27.28 mm, and that of new model is 43.28 mm. Another difference concerns the blade thickness. For the original model, the blade thickness is always kept at 12% of the blade length. To describe the change in blade thickness, a parameter which named *blockage ratio* is defined. The definition of the blockage ratio is shown in Equation (1),

$$B = \frac{2\pi r - z \frac{t}{\sin \theta}}{2\pi r} \times 100\% \quad (1)$$

In Equation (1), B represents the blockage ratio, r represents the radius of the rotor, z represents the blade number of the rotor, t represents the blade thickness, θ represents the setting angle of the blade. We can observe from the equation that the blade thickness will become smaller with increasing blockage ratio. If the blade thickness decreases, the flow passage between the near two blades will be expanded, that means the flow passage will become wider. Because the blade thickness of the original model was always 12%, the blockage ratio of the original model increases during the radial direction.

We adopted a new method to design the blade of the new model. This method involves keeping the blockage ratio constant in the radial direction. According to the new method, the blade thickness

is not always kept constant. Instead of a constant value, we want to decrease the blade thickness, and also make the flow passage wider than in the original model. We choose the smallest blockage ratio and applied it to the whole radial direction. Therefore, the blockage ratio is the same during the radial direction. The blockage ratio of the new model and the other detailed parameters are shown in Table 2. To compare with the new model, the original blockage ratio and blade thickness of the front and rear rotors are also shown in Table 2.

Table 2. The new blockage ratio and blade thickness of the front and rear rotor.

R (mm)	Blade Thickness Over Blade Length of Original Model (%)	Blade Thickness Over Blade Length of New Model (%)	Original Blockage Ratio of Front Blade (%)	New Blockage Ratio of Front Blade (%)	Original Blockage Ratio of Rear Blade (%)	New Blockage Ratio of Rear Blade (%)
29	12	12	90.52	90.52	92.89	92.89
26.1	12	11.44	90.05	90.52	92.54	92.89
23.2	12	10.8	89.46	90.52	92.10	92.89
20.3	12	10.08	88.71	90.52	91.53	92.89
17.4	12	9.26	87.71	90.52	90.78	92.89
14.5	12	8.31	86.30	90.52	89.73	92.89

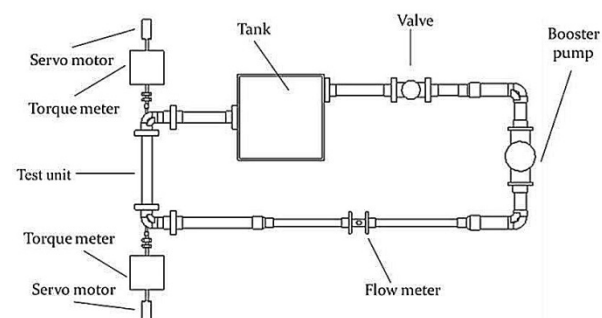
The working environment of the contra-rotating small hydro-turbine is a small water supplying casing. In order to support the small hydro-turbine inside the casing, a spacer which includes 4 spokes around it was designed. In the future, the generators are planned to be put inside of the front and rear hubs, and the rotors will be supported only by the spokes. The spacer is between the front and rear rotors; its diameter is 29 mm, with both the front and rear hubs. The length of the spacer is 33 mm.

2.2. Experimental Apparatus and Method

To perform experiments for this contra-rotating small hydro-turbine, an experimental apparatus is assembled. A photo of the experimental apparatus is shown in Figure 2a. The schematic diagram of the apparatus is shown in Figure 2b. The test turbine was installed inside the test section casing, which was transparent for visualization. The casings were filled with water. To obtain the head, we used two pressure sensors to measure the pressure differences between the two-dimensional (2D) upstream of the front rotor and the 2D downstream of the rear rotor. In these experiments, the rotors were driven by two servo motors. The servo motors are assembled beside the test section. To make sure that the influence of the swirl flow from the elbow is suppressed, the length of the test section was 500 mm, i.e., long enough to suppress interference.



(a)



(b)

Figure 2. The experimental apparatus of contra-rotating small hydro-turbine: (a) Photo of experimental apparatus, the flow direction is clockwise; (b) Schematic diagram of the experimental apparatus.

We used a magnetic flow meter KEYENCE FD-UH50H (Keyence, Osaka, Japan) to measure the flow rate Q inside the casing. The flow meter is installed far from the test turbine to separate it from the wake from the test turbine. The accuracy of the flow meter is $\pm 0.5\%$. We also used a torque meter ONO SOKKI SS050 (ONO SOKKI, Yokohama, Japan) to measure the torque of the rotors; the accuracy of the torque meter is $\pm 0.5\%$. The rotation speed of the rotor was measured with a rotation speed sensor ONO SOKKI MP-981 (ONO SOKKI, Yokohama, Japan). We used the data obtained by the sensors to calculate the performance of the contra-rotating small hydro-turbine. For example, we used the torque to calculate the shaft power; the ratio of shaft power to the water power gives the hydraulic efficiency.

3. Numerical Analysis Conditions

ANSYS-CFX (16.2, ANSYS, Pittsburgh, PA, USA) was used as the numerical simulation software. We made this numerical simulation under 3D unsteady flow conditions. We assumed that the fluid media is incompressible, isothermal water. The finite volume method was used in ANSYS-CFX. We chose stand $k-\varepsilon$ as the turbulence model because it is proven to be accurate in engineering calculations. We also use the standard wall function near the wall. Therefore, the accuracy of the calculations can be ensured.

The numerical grids of the whole domains in ANSYS-CFX are shown in Figure 3a, and the grids data of the test rotors connected with spacers are shown in Figure 3b.

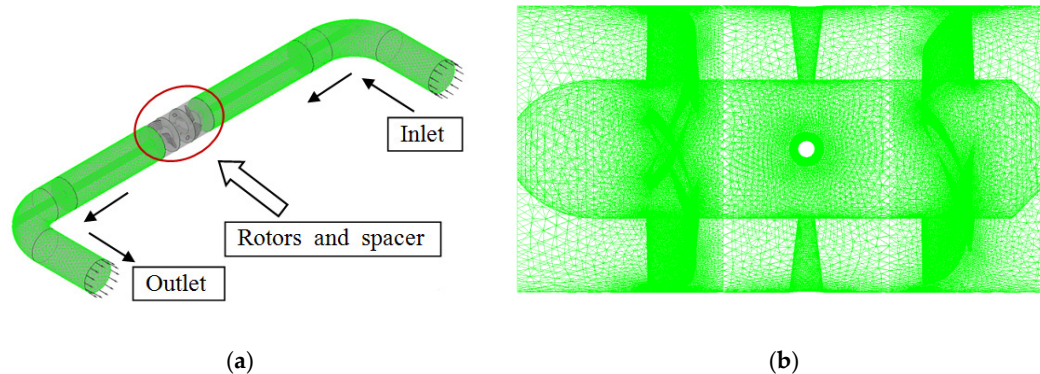


Figure 3. The numerical simulation model of contra-rotating small hydro-turbine: (a) Numerical grids of the whole domains; (b) Mesh data of test turbine, the flow direction is from left to right.

The numerical analysis model is designed to be the same with test section. We designed the inlet and outlet elbows in the simulation model. The test section is long enough to be same with the experimental apparatus, and the influence of the elbow can be also suppressed in the numerical simulation. The driving shafts were also removed from the flow passage in the numerical simulation to match those of the experimental apparatus. The front and rear rotors rotate in the contrary direction in the numerical simulation. The numerical simulation consists of 3 steps: the first is a steady simulation; the second is transient simulation whose initial value is the result of the first step; the third step is outputting the result.

The inlet boundary condition is constant mass flow and the outlet boundary condition is constant pressure in the numerical simulation. We also set up the interface between each domain. During the unsteady simulation, the number of time-steps per revolution is 120. Therefore, the time step is $t_s = 2.174 \times 10^{-4}$ s. We established 7 parts in the numerical simulation. They are: inlet elbow, inlet casing, front rotor, spacer, rear rotor, outlet casing, and outlet elbow. The grid number is suitable for this simulation. The total number of grids for the whole numerical simulation is about 7,000,000. We chose a blade area to refine the mesh because the blade involves complicated geometry for which the physical quantity is changed a lot at the blade area. We refined all blades in the front and rear rotors, and defined the maximum grid size of this refinement area at 0.35 mm. Therefore, the grid at

the blade area is refined. We set up an inflation layer on the outside surface of the rotor. The thickness of this inflation layer is 1mm. Regarding the value of y^+ , it was less than 100 and bigger than 50 at most of the domains. The maximum of y^+ is 230 at a small area which was difficult to mesh. We choose 13 flow rate points to make the numerical simulations; the flow rates ranged from 90% to 200% of the design flow rate.

4. Results and Discussions

4.1. Experimental Results of Original Model and New Model

To prove the accuracy of the numerical simulation, we undertook performance experiments for the original model and new model. The process of the experiment is shown in Figure 4. In Figure 4, the rotation speed is 2300 r/min, and the test section is full of water.



Figure 4. The picture of the experiment process, the flow direction is from left to right.

During the experiments, we mainly measured the torque and pressure. Torque was measured by the torque meters connected with the driving shafts. The pressure was measured by pressure sensors installed 2D upstream of the front rotor and 2D downstream of the rear rotor. By the torque and pressure, we could calculate the power, head and efficiency of this contra-rotating small hydro-turbine. The experiment results of original and new models were compared to prove the accuracy of the simulation. Comparisons are shown in Figure 5a,b.

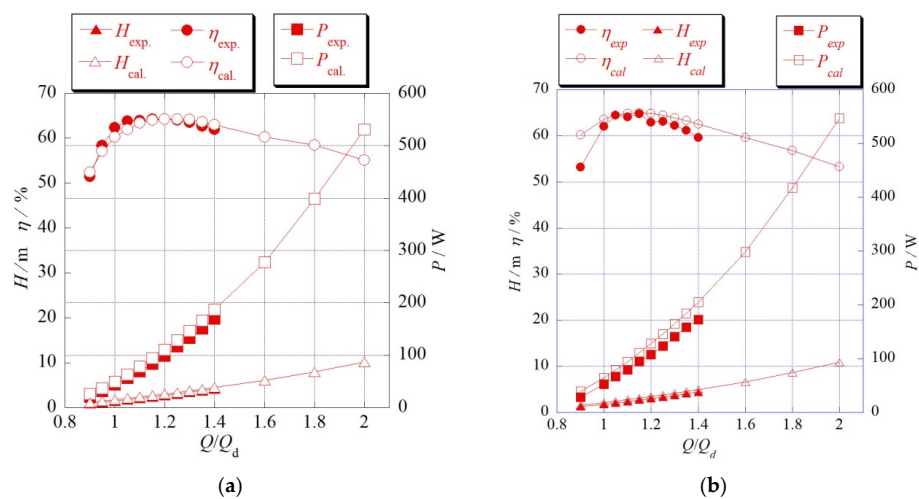


Figure 5. Comparison between experiment result and numerical result. (a) Comparison of the original model. (b) Comparison of the new model.

In Figure 5a,b, the horizontal axis is flow rate ratio between present flow rate Q and design flow rate Q_d . The first vertical axis is head and efficiency of the test turbine. The second vertical axis is the power of test turbine. The flow meter has range limitation. Therefore, the maximum flow rate in the experiments was $Q = 1.4 \times Q_d$. From the comparisons in Figure 5a,b, we can observe that the numerical and experimental results are well-matched. The experimental results show that the numerical simulation can reflect the performance of the contra-rotating small hydro-turbine. Therefore, the numerical result was shown to be correct, and we could use the numerical result to investigate and analyze the internal flow conditions of the original and new models.

4.2. Investigation and Analysis on the Attack Angle

Because the numerical simulation was proven to be correct, we used the simulation results to obtain the axial velocity and circumferential velocity on different planes and different points. Then we used the axial velocity and circumferential velocity to calculate the attack angle of that point. By means of observing the changing rule of the axial velocity, circumferential velocity, and attack angle, we could further enhance our comprehension to the internal flow conditions of this contra-rotating small hydro-turbine.

In order to obtain the velocity and attack angle at a suitable position, we established two planes in front of the front and rear rotors. One of the planes was 3 mm upstream from the front rotor. The other was 3 mm upstream of the rear rotor. Choosing 3 mm is an attempt to find a suitable position to reflect the velocity distribution and attack angle. In each plane, we established 6 points and output the axial velocity and circumferential velocity. The 6 points were in different section planes of the blade, and the section planes change from the bottom to the top of the blade. We set up 6 points to observe the velocity distribution and attack angle because the blade is established based on six 2D blade profiles. Then, the attack angle could be calculated by the axial velocity and circumferential velocity. The axial velocity of the original model 3 mm upstream of the front rotor is shown in Figure 6a, and the circumferential velocity of the original model 3 mm upstream of the front rotor is shown in Figure 6b.

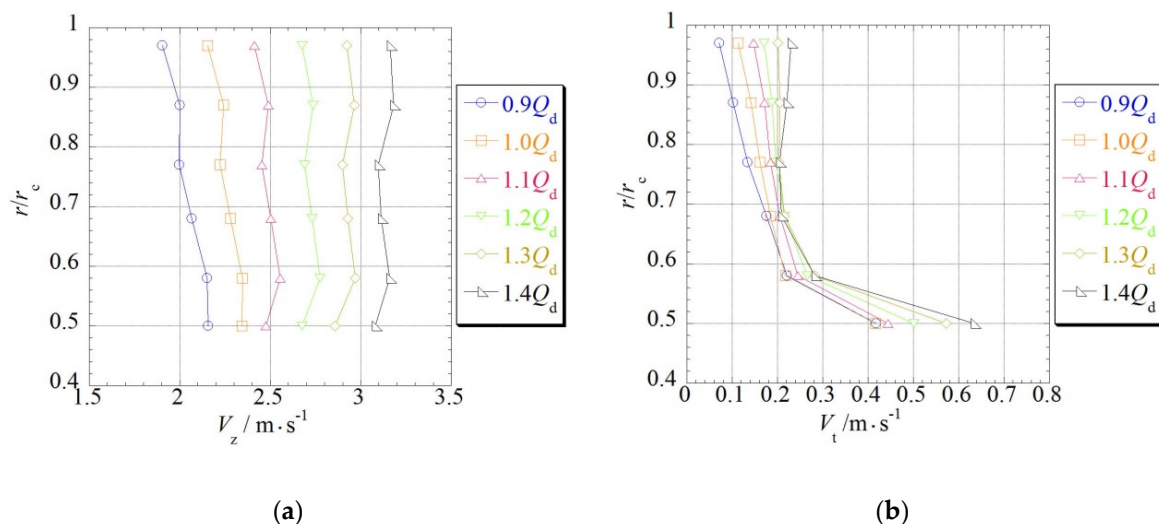


Figure 6. The front rotor axial velocity and circumferential velocity of original model: (a) Axial velocity; (b) Circumferential velocity.

In Figure 6a,b, the X axis is axial velocity, the Y axis is the ratio between present radius r and radius of the casing r_c . This will help to clarify the value distribution on different sections of the blade. In Figure 6a, we can observe that the axial velocity of the original model 3 mm upstream the front rotor was not significantly changed across different sections, and the axial velocity increased with increasing flow rate. From Figure 6b, we can observe that the circumferential velocity of the original

model 3 mm upstream the front rotor is changed a lot in different sections when the radius decreases and the circumferential velocity increases. That means that the rotational motion of the water near the hub of the front rotor is more intense.

The axial velocity of the original model 3 mm upstream of the rear rotor is shown in Figure 7a, and the circumferential velocity of the original model 3 mm upstream of the rear rotor is shown in Figure 7b. From Figure 7a, we can observe that the axial velocity of the original model 3 mm upstream the rear rotor has changed after the water passed through the front rotor and spacer. The changing range of the axial velocity became wider when the flow rate became larger. Notably, the axial velocity near the hub of the rotor is negative, meaning that backflow will occur when the flow rate is high enough. The circumferential velocity upstream the rear rotor became large in the center field of the blade; this is obvious with the increased flow rate.

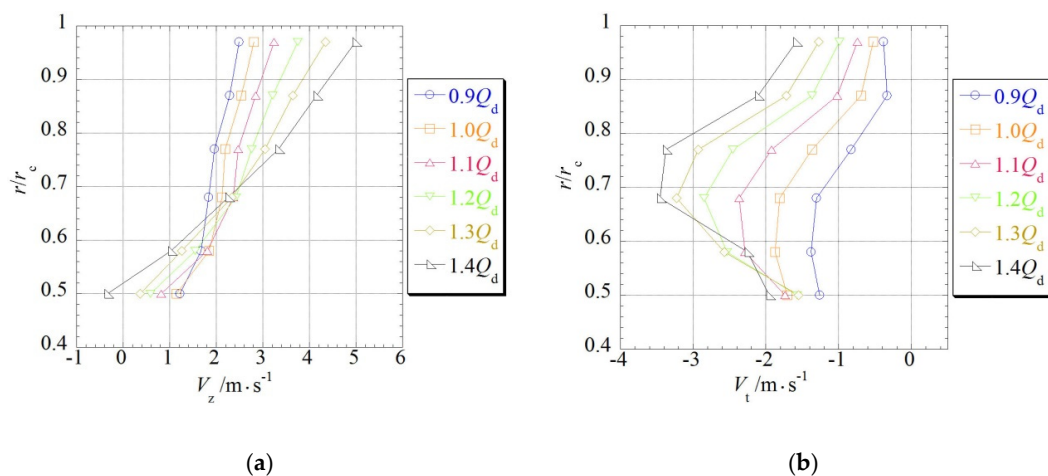


Figure 7. The rear rotor axial velocity and circumferential velocity of original model. (a) Axial velocity. (b) Circumferential velocity.

The attack angle is a key parameter to the small hydro-turbine because the performance will change with the changing of attack angle. The position of the attack angle is shown in Figure 8. From Figure 8, we can see that the attack angle can be calculated by the inlet and setting angles. The setting angle was confirmed when we finished designing, and the inlet angle could be calculated by the axial velocity and circumferential velocity.

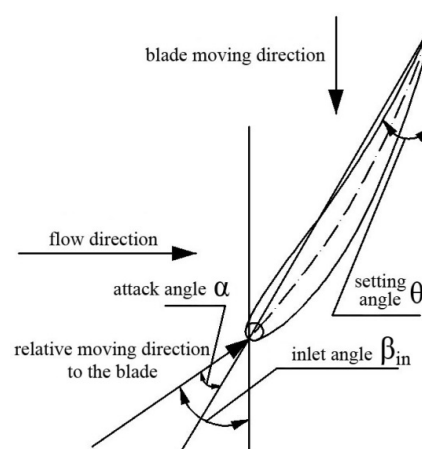


Figure 8. The position of the attack angle.

Therefore, firstly, we can use the axial velocity and circumferential velocity to calculate the inlet angle. Then we can use the inlet angle and setting angle to calculate the attack angle. The inlet angle can be calculated as following Equation (2),

$$\beta_{in} = \tan^{-1} \left(\frac{V_z}{|u - |V_t||} \right) \quad (2)$$

In Equation (2), β_{in} denotes the inlet angle, V_z denotes the axial velocity, V_t denotes the circumferential velocity, u denotes the velocity of the blade. u can be calculated as the following Equation (3):

$$u = r \times 2\pi \times \frac{2300}{60} \quad (3)$$

In Equation (3), u denotes the velocity of the blade. r denotes the section located radius. After obtaining the inlet angle, we can calculate the attack angle. The attack angle can be calculated as the following Equation (4):

$$\alpha = \beta_{in} - \theta \quad (4)$$

In Equation (4), α denotes the attack angle, β_{in} denotes the inlet angle, θ denotes the setting angle. The attack angle of original model 3 mm upstream the front rotor is shown in Figure 9a, the attack angle of original model 3 mm upstream the rear rotor is shown in Figure 9b.

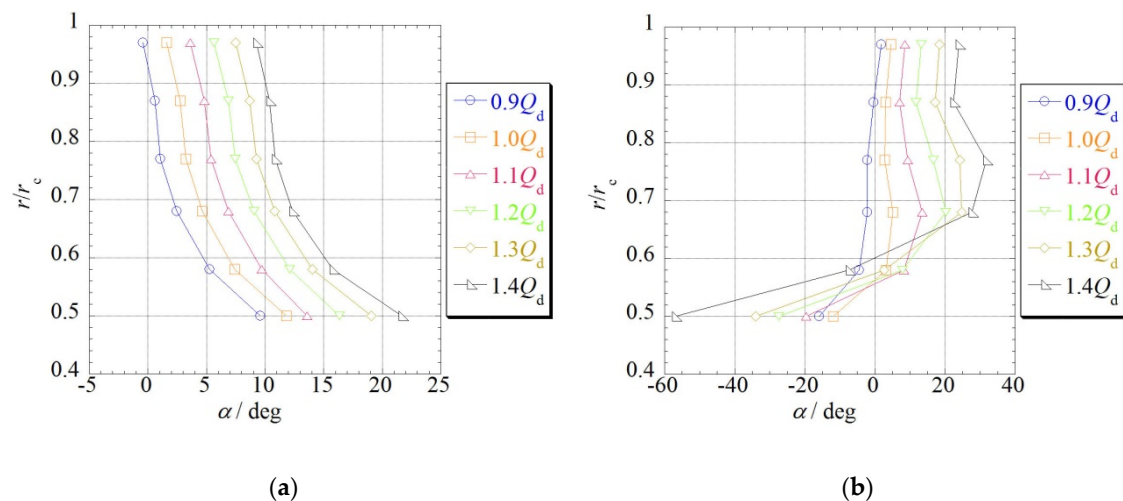


Figure 9. The attack angle of original model: (a) Upstream the front rotor; (b) Upstream the rear rotor.

From Figure 9a, we can observe that the attack angle of the original model increases with the decreasing radius. That means the attack angle is larger at the hub area. With an increasing flow rate, the distribution of the attack angle is not significantly changed; the curve is just moved to right side. Therefore, the attack angle upstream of the front rotor will not be highly influenced by the changing flow rate. However, the changing rule of the attack angle upstream of the rear rotor is quite different to that of the front rotor. From Figure 9b, we can observe that the attack angle upstream of the rear rotor is highly influenced by the changing of the flow rate. When the flow rate increases, the attack angle near the hub area is acutely decreased, resulting in the big difference of attack angle between the tip area and hub area. This phenomenon reflects that the flow condition in front of the rear rotor is quite confused and complicated, and the flow condition in front of the rear rotor has a big difference near the hub and tip areas. A big attack angle will also result in unstable running of the small hydro-turbine. Therefore, the attack angle in front of the rear rotor will have a deep impact on performance.

Because the computational fluid dynamics (CFD) simulation of the new model has been proven to be correct by the experiments, we can use the numerical result to investigate the attack angle of the new model. The axial velocity of the new model 3 mm upstream of the front rotor is shown in Figure 10a, and the circumferential velocity of the new model 3 mm upstream of the front rotor is shown in Figure 10b. From Figure 10a, we can observe that the axial velocity of the new model has a different changing rule compared with the original model. The axial velocity of the new model becomes smaller at the hub area, while it is bigger at the middle area compared with the original model. Therefore, the modification of the blade thickness and front hub result in the difference of the front axial velocity between new model and original model. This difference of the front axial velocity will also result in the difference of the rear flow conditions. From Figure 10b, we can observe that the circumferential velocity at hub area is larger than that of the original model. That means rotational movement is stronger than that of the original model.

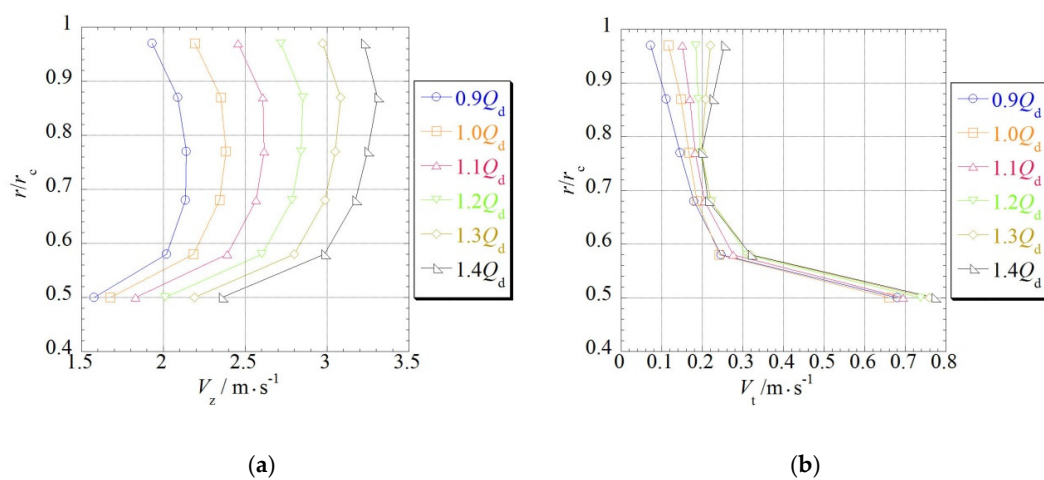


Figure 10. The front rotor axial velocity and circumferential velocity of new model: (a) Axial velocity; (b) Circumferential velocity.

The axial velocity of the new model 3 mm upstream of the rear rotor is shown in Figure 11a. The circumferential velocity of the new model 3 mm upstream of the rear rotor is shown in Figure 11b.

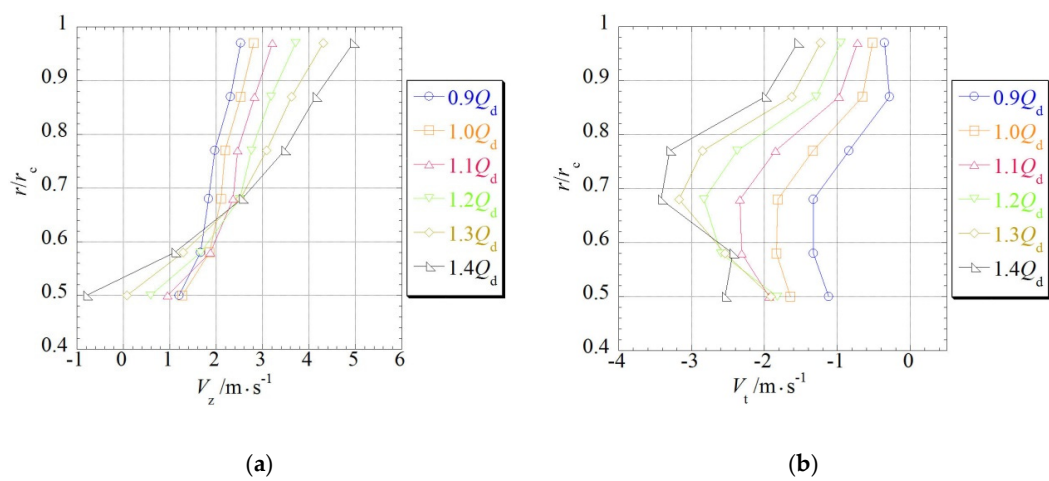


Figure 11. The rear rotor axial velocity and circumferential velocity of new model: (a) Axial velocity; (b) Circumferential velocity.

From Figure 11a,b, we can observe that the axial velocity and circumferential velocity of the rear rotor become larger than those of the original model, especially in the large flow rate status. The attack angle in front of the rear rotor can be also calculated by the same method.

The attack angle of the new model 3 mm upstream of the front rotor is shown in Figure 12a, and the attack angle of the new model 3 mm upstream of the rear rotor is shown in Figure 12b. From Figure 12a, we can observe that the attack angle of the new model 3 mm upstream of the front rotor has obvious differences compared with the original model. The attack angle of the new model is smaller at the hub area. Therefore, the new front hub helps to decrease the front attack angle. This phenomenon proves that the flow direction is vertical to the front blade in the new model. That's why we changed the shape of the front hub; the attack angle can reflect that we have achieved our goal. By means of changing the front attack angle, the rear flow condition is changed, and the performance of this contra-rotating small hydro-turbine is further improved. From Figure 12b, we can observe that the attack angle of the new model 3 mm upstream of the rear rotor is also changed at the hub area. When the flow rate increases, the attack angle of the new model 3 mm upstream of the rear rotor is much smaller than that of the original model. This is mainly because of the changing of front attack angle at hub area.

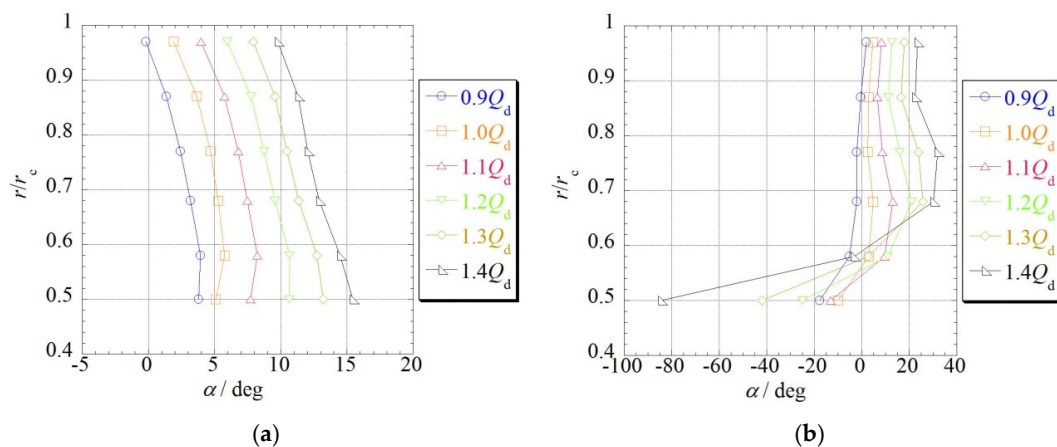


Figure 12. The attack angle of new model: (a) Upstream the front rotor; (b) Upstream the rear rotor.

4.3. Investigation and Analysis on the Rear Flow Condition

We are interested in the rear flow conditions because a lot of evidence supports the hypothesis that the rear rotor is key to enhancing the performance of the contra-rotating small hydro-turbine. Therefore, some differences of the rear flow conditions between the original and new models were investigated. Pressure distributions of the original and new models in viewpoint of blade to blade are shown in Figure 13.

In Figure 13, the flow rate of original model is $1.2 \times Q_d$, and the flow rate of new model is $1.15 \times Q_d$; these are their highest efficiency flow rates. The radius position is $r/r_c = 0.85$, r represents the present radius, and r_c represents the radius of the casing. The left side is the pressure distribution of the original model. The right side is the pressure distribution of the new model. The middle pictures are the stagnation points of the original model new models. From Figure 13, we can observe that there are low-pressure areas behind the blades and spokes. That means that the flow separation happens in these areas. For the original model, the low-pressure areas are big and connected with the spoke. For the new model, the low-pressure areas are suppressed, and internal flow conditions are improved. We focused on the rear flow conditions because the rear rotor is the key point. When we investigated the details of rear flow conditions, we found that the rear rotor's stagnation points in the original model and the new model are different. Compared with the original model, the rear rotor's stagnation point in the new model is moved downward to the pressure surface of the rear blade. Because of this change of stagnation point, the new model's separation at the leading edge area is suppressed,

while the original model's separation at the leading area is expanded in the cascade frontal line. Finally, the separation in the leading edge area is suppressed, and the rear flow conditions are improved.

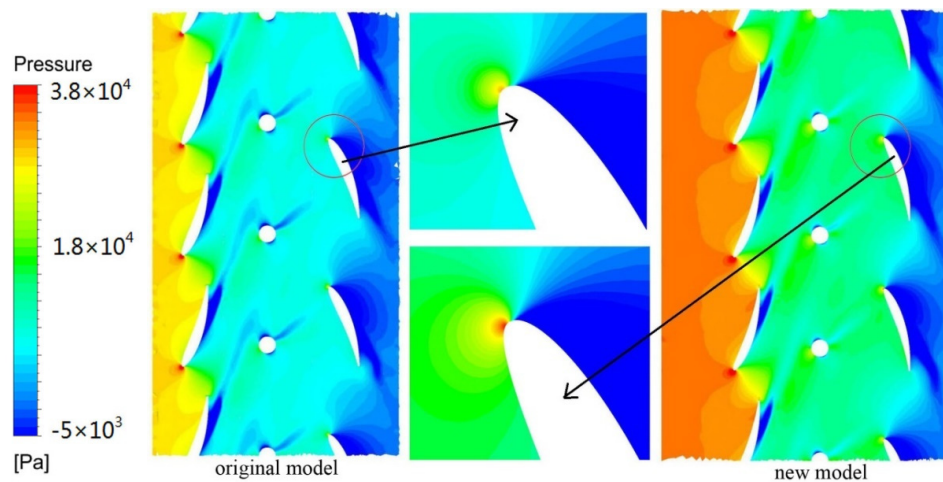


Figure 13. Pressure distributions of the original model and new model in their each highest efficiency.

We are also interested in the rear flow condition at the tip clearance area, because tip clearance is very important parameter and has a great influence on the performance of the contra-rotating small hydro-turbine. To clarify the flow condition at tip clearance area, we set a plane at the middle of the tip clearance area and unfolded the streamlines at that plane. The tip clearance of this contra-rotating small hydro-turbine is 1mm; therefore, the plane is 0.5 mm away from the tip of the rear blade. We also showed the pressure distribution of the rear blade to illuminate the flow conditions at the rear tip clearance area. The pressure distribution of the rear blade and the streamlines at rear tip clearance area are shown in Figure 14.

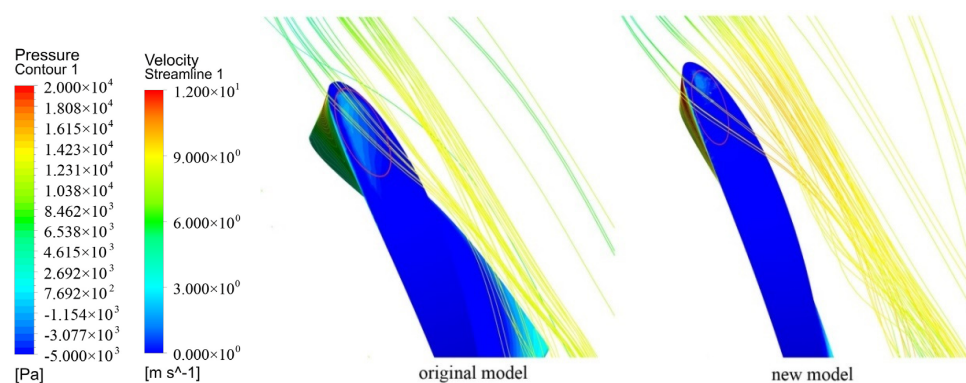


Figure 14. Pressure distributions of rear blade and streamlines at rear tip clearance area.

From Figure 14, we can observe the difference in pressure distribution, here emphasized by the red circle. We can find that the original model's pressure at the tip clearance area is higher than that of the new model. That means the flow is more crowded at the tip clearance of the original model. This is not a good phenomenon, because the turbulent kinetic energy after the front rotor can't be released and fully taken up by the rear rotor. A part of turbulent kinetic energy is changed to pressure potential energy and can't be used to output the torque of rear rotor. This problem is solved in the new model. The pressure at tip clearance area is decreased and the flow is smooth. The turbulent kinetic energy can be fully used to output the torque of the rear rotor. This flow condition can also be proven by the

streamlines on the right side of the rear blade. From the streamlines, we can find that the velocity of the new model is bigger than that of the original model. The streamlines of new model also show that the flow is more chaotic because the streamlines are more confused and have spiral flow characteristics. The turbulent kinetic energy is in direct proportion to the velocity and Reynolds number. Therefore, the new model's turbulent kinetic energy at the rear rotor area is bigger than that of the original model.

The turbulent kinetic energy distribution of the original model and new model on the rear blades are shown in Figure 15. From Figure 15, we can see that the position of high turbulent kinetic energy of the new model is different to that of the original model. For the original model, the high turbulent kinetic energy area acts on the top of the rear blade, while the high turbulent kinetic energy area of the new model is moved forward to the middle of the blade. This also demonstrates that the flow of new model at the tip clearance area is smooth because the chaotic flow in front of the rear rotor is moved from the top to the middle area of the blade. High turbulent kinetic energy can help to drive the rear rotor and enhance the outputting torque of the rear rotor. Therefore, the changing of the high turbulent kinetic energy area will help to enhance performance.

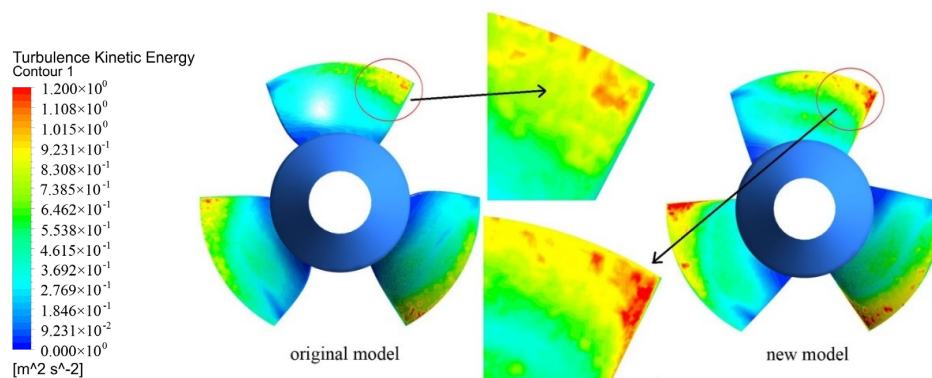


Figure 15. The rear blade's turbulent kinetic energy distributions of original and new models.

If we can determine the rotating angles when the rotors are rotating, it is be convenient for us to investigate the internal flow conditions by the rotating angles. Therefore, two angles are defined as θ_f and θ_r . At the beginning of the design, a base line is defined to separate the blade into two parts. The blade is separated for 25% and 75% of the chord; we chose this base line as the meridional plane. We also defined this as the beginning position of the rotation. The two angles will be changed with the rotation of the front and rear rotors. Therefore, the angle θ_f is defined as the angle between the base line of front blade and the meridional plane. The angle θ_r is defined as the angle between base line of rear blade and the meridional plane. A schematic diagram of the two angles is presented in Figure 16.

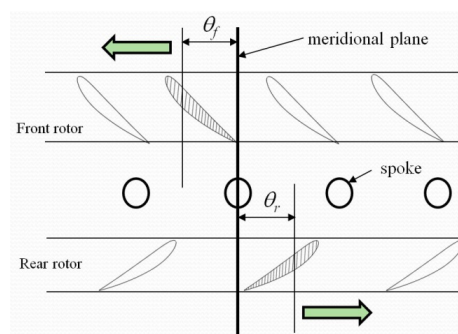


Figure 16. The schematic diagram of rotating angle.

At the beginning, we defined $\theta_f = 0^\circ$ and $\theta_r = 0^\circ$. This causes the base line of the front rotor and that of the rear rotor to be coincident with the meridian plane. The rotors rotate 3° in each time-step. Then, θ_f and θ_r become $\theta_f = 3^\circ$ and $\theta_r = -3^\circ$ in the next time-step. The θ_r is defined as negative because the rear rotor rotates in the opposite direction to the front rotor. The rotating direction of the front rotor is defined as positive, and that of the rear rotor as negative.

A comparison between the rear rotor's torque of the original and new models is shown in Figure 17. From Figure 17, we can see that rear rotor's torque for the new model is bigger than that of original model, and the torque of rear rotor is changed smoothly at the top and bottom of the curve. Therefore, the torque of the rear rotor is enhanced, and rear flow conditions are improved.

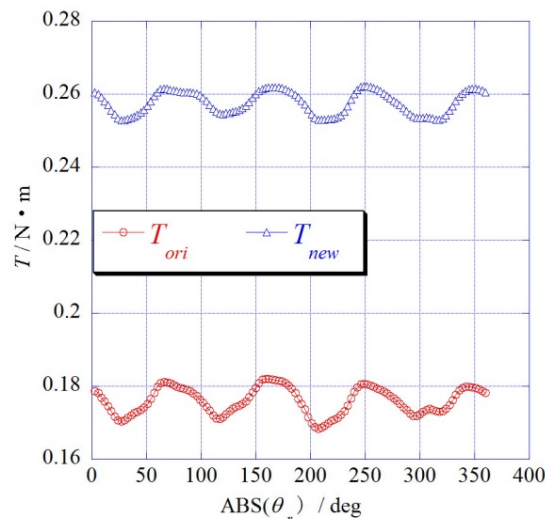


Figure 17. Comparison between the rear rotor's torque.

5. Conclusions

In this paper, the attack angle and rear flow conditions of the contra-rotating small hydro-turbine were investigated and analyzed. Two planes are created, located 3 mm upstream of the front rotor and 3 mm upstream of the rear rotor. The attack angle of the original and new models were compared. The rear flow conditions of the original and new models are also investigated. The rear flow details, such as the movement of the stagnation point, the pressure distribution, streamlines at tip clearance area, and the turbulent kinetic energy distribution on the rear blade, are clarified. The rear torque of the original and new models were also compared to support the investigation and analysis. According to the results, we can draw the following conclusions:

- The contra-rotating small hydro-turbine can be installed in water supplying systems in farmland settings, and remote rural areas can use the electrical power which is generated by this system. Besides, some support structures like guide vanes or fairwater can be used in this hydro-turbine. These support structures can help to improve the flow conditions. However, to make this contra-rotating small hydro-turbine as compact as possible, we did not adopt guide vanes and fairwater. We designed a spacer which includes four spokes to support the contra-rotating small hydro-turbine in the casing.
- The attack angle of the new model is smaller at the hub area. Therefore, the new front hub helps to decrease the front attack angle. This phenomenon proves that water can flow into the front blade more directly. It was for this reason that we changed the shape of the front hub; the attack angle demonstrates that we have achieved our goal. By means of changing the front attack angle, the rear flow condition is changed, and the performance was further improved.

- Compared with the original model, the rear rotor's stagnation point in new model is moved downward to the pressure surface of the rear blade. Because of this change to the stagnation point, the new model's separation at the leading edge area is suppressed, while the original model's separation at leading edge area is expanded in the cascade frontal line. Therefore, this change to the stagnation point helped to suppress separation at the leading edge area and improve the rear flow conditions.
- The flow is more crowded at the tip clearance of the original model by reflections of the pressure distribution at tip clearance area. The turbulent kinetic energy is changed to pressure potential energy and can't be used to output the torque of the rear rotor. This problem is resolved in the new model, because pressure at the tip clearance area is decreased and the flow is smooth. This can also be demonstrated by the streamlines of original and new models. The high turbulent kinetic energy area of the new model is moved forward, to the middle of the blade. The rear rotor's torque in the new model is greater than that of original model, and the torque of rear rotor is changed smoothly at the top and bottom of the curve. Therefore, the torque of the rear rotor is enhanced, and rear flow conditions are improved.

Author Contributions: D.N. obtained the experimental and numerical results and finished the manuscript of this paper, T.S. and S.Z. made correction to this paper and gave some useful suggestions.

Funding: This research was funded by Japan Science and Technology Agency (No. AS262Z00175L), KEIRIN RACE (No. 27–176, No. 28–125), Japan Society for the Promotion of Science (No. 24760138, No. 16K18017).

Acknowledgments: This research was supported by Adaptable and Seamless Technology Transfer Program (No. AS262Z00175L) through Targetdriven R&D from J.S.T., JKA and its promotion funds from KEIRIN RACE (No. 27–176 and No. 28–125), the Awa Bank Science and Culture Foundation, the Grant-in-Aid for Young Scientists (B) from Japan Society for the Promotion of Science No. 24760138, No. 16K18017, TEPCO Memorial Foundation and Hatakeyama Culture Foundation. We would like to show our special thanks for the foundations.

Conflicts of Interest: The authors declare no conflict of interest.

Nomenclature

Q_d	Design flow rate of the small hydro-turbine
H_d	Design head of the small hydro-turbine
P_a	Power assumed in a pipe of agricultural water
H_a	Head assumed in a pipe of agricultural water
Q_a	Flow rate assumed in a pipe of agricultural water
Q	Flow rate in the experimental apparatus
H_{df}	Design head of front rotor
H_{dr}	Design head of rear rotor
N_f	Rotation speed of front rotor
N_r	Rotation speed of rear rotor
D	The diameter of the casing
D_{hf}	The hub diameter of front rotor
D_{if}	The tip diameter of front rotor
D_{hr}	The hub diameter of rear rotor
D_{tr}	The tip diameter of rear rotor
Z_f	Blade number of front rotor
Z_r	Blade number of rear rotor
B	The blockage ratio of the blade
r	Present radius of the front or rear rotor
Z	Blade number of the front or rear rotor
t	The thickness of front or rear blade
θ	The setting angle of front or rear blade
t_s	The time-step in the numerical analysis
r_c	The radius of the casing

α	The attack angle
u	The velocity of the blade
β_{in}	The inlet angle
V_z	The axial velocity
V_t	The circumferential velocity
θ_f	Base line angle of front rotor
θ_r	Base line angle of rear rotor

References

1. Scott, C.A.; Sugg, Z.P. Global energy development and climate-induced water scarcity—Physical limits, sectoral constraints, and policy imperatives. *Energies* **2015**, *8*, 8211–8225. [[CrossRef](#)]
2. Furukawa, A.; Okuma, K.; Tagaki, A. Basic study of low head water power utilization by using darrieus-type turbine. *Trans. JSME* **1998**, *64*, 2534–2540. [[CrossRef](#)]
3. Kanemoto, T.; Inagaki, A.; Misumi, H.; Kinoshita, H. Development of Gyro-type hydraulic turbine suitable for shallow stream (1st Report, rotor works and hydroelectric power generation). *Trans. JSME* **2004**, *70*, 413–418. [[CrossRef](#)]
4. Kei, T.; Kotaro, H.; Kai, S.; Satoshi, W.; Daisuke, M.; Akinori, F. A study on darrieus-type hydro-turbine toward utilization of extra-low head natural flow streams. *Intern. J. Fluid Mach. Syst.* **2013**, *6*, 152–159. [[CrossRef](#)]
5. Daisuke, M.; Kei, T.; Satoshi, W.; Kusuo, O.; Akinori, F. Experimental and numerical investigations on performances of darrieus-type hydro-turbine with inlet nozzle. *Intern. J. Fluid Mach. Syst.* **2014**, *7*, 151–159. [[CrossRef](#)]
6. Matsui, J. Internal flow and performance of the spiral water turbine. *Turbomachinery* **2010**, *38*, 358–364.
7. Ikeda, T.; Iio, S.; Tatsuno, K. Performance of nano-hydraulic turbine utilizing waterfalls. *Renew. Energy* **2010**, *35*, 293–300. [[CrossRef](#)]
8. Nakajima, M.; Iio, S.; Ikeda, T. Performance of savonius rotor for environmentally friendly hydraulic turbine. *J. Fluid Sci. Technol.* **2008**, *3*, 420–429. [[CrossRef](#)]
9. Iio, S.; Uchiyama, F.; Sonoda, C.; Ikeda, T. Performance improvement of savonius hydraulic turbine by using a shield plate. *Turbomachinery* **2009**, *37*, 743–748.
10. Iio, S.; Oike, S.; Sato, E.; Ikeda, T. Failure events in the field text of environmentally friendly nano-hydraulic turbines. *Turbomachinery* **2011**, *39*, 162–168.
11. Kanemoto, T.; Kaneko, M.; Tanaka, D.; Yagi, T. Development of counter-rotating type machine for water power generation (1st Report, counter-rotating type generator and axial-flow runners). *Trans. JSME* **2000**, *66*, 1140–1146. [[CrossRef](#)]
12. Kanemoto, T.; Tominaga, K.; Tanaka, D.; Sato, T.; Kashiwabara, T.; Uno, M. Development of counter-rotating type machine for hydroelectric power generation (2nd Report, hydraulic performance and potential interference of counter-rotating runners). *Trans. JSME* **2002**, *68*, 3416–3423. [[CrossRef](#)]
13. Tanaka, D.; Kanemoto, T. Development of counter-rotating type machine for hydroelectric power generation (3rd Report, design materials for solidity of axial flow runners). *Trans. JSME* **2006**, *72*, 686–692. [[CrossRef](#)]
14. Creech, A.C.W.; Borthwick, A.G.L.; Ingram, D. Effects of support structures in an LES actuator line model of a tidal turbine with contra-rotating rotors. *Energies* **2017**, *10*, 726. [[CrossRef](#)]
15. Shigemitsu, T.; Fukutomi, J.; Tanaka, C. *Renewable Energy in the Service of Mankind*; Springer International Publishing: Cham, Switzerland, 2015; Volume I.
16. Sonohata, R.; Fukutomi, J.; Shigemitsu, T.T. Study on the contra-rotating small-sized axial flow hydro turbine. *Open J. Fluid Dyn.* **2012**, *2*, 318–323. [[CrossRef](#)]
17. Shigemitsu, T.; Fukutomi, J.; Sonohata, R. Performance and internal flow of contra-rotating small hydro turbine. In Proceedings of the ASME Fluids Engineering Division Summer Meeting, Incline Village, NV, USA, 7–11 July 2013.
18. Shigemitsu, T.; Fukutomi, J.; Tanaka, C. Unsteady flow condition of contra-rotating small-sized hydro turbine. In Proceedings of the 12th Asian International Conference on Fluid Machinery, Yogyakarta, Indonesia, 25–27 September 2013.

19. Shigemitsu, T.; Takeshima, Y.; Tanaka, C.; Fukutomi, J. Influence of spoke geometry on performance and internal flow of contra-rotating small-sized hydroturbine. In Proceedings of the ASME/JSME/KSME Joint Fluids Engineering Conference, Seoul, Korea, 26–31 July 2015.
20. Nan, D.; Shigemitsu, T.; Zhao, S.D.; Takeshima, Y. Numerical analysis of contra-rotating small hydro-turbine with cylinder spoke. *Int. J. Fluid Mach. Syst.* **2018**, *11*, 21–29. [[CrossRef](#)]
21. Nan, D.; Shigemitsu, T.; Zhao, S.D.; Takeshima, Y. Internal flow and performance with foreign vegetable materials in a contra-rotating small hydro-turbine. *Int. J. Fluid Mach. Syst.* **2017**, *10*, 385–393. [[CrossRef](#)]
22. Nan, D.; Shigemitsu, T.; Zhao, S.D.; Ikebuchi, T.; Takeshima, Y. Study on performance of contra-rotating small hydro-turbine with thinner blade and longer front hub. *Renew. Energy* **2018**, *117*, 184–192. [[CrossRef](#)]
23. Gabl, R.; Innerhofer, D.; Achleitner, S.; Righetti, M.; Aufleger, M. Evaluation criteria for velocity distributions in front of bulb hydro turbines. *Renew. Energy* **2018**, *121*, 745–756. [[CrossRef](#)]



© 2018 by the authors. Licensee MDPI, Basel, Switzerland. This article is an open access article distributed under the terms and conditions of the Creative Commons Attribution (CC BY) license (<http://creativecommons.org/licenses/by/4.0/>).